ARTICLE

Revealing the Influence of Molecular Chemisorption Direction on the Reaction Selectivity of Dehalogenative Coupling on Au(111): Polymerization versus Cyclization

Zewei Yi, Zhaoyu Zhang, Yuan Guo, Yuhong Gao, Rujia Hou, Chi Zhang,* Yousoo Kim,* and Wei Xu*

ACCESS | Metrics & More | Article Recommendations | Supporting Information

ABSTRACT: The control of reaction selectivity is of great interest in chemistry and depends crucially on the revelation of key influencing factors. Based on well-defined molecule−substrate model systems, various influencing factors have been elucidated, focusing primarily on the molecular precursors and the underlying substrates themselves, while interfacial properties have recently been shown to be essential as well. However, the influence of molecular chemisorption direction on reaction selectivity, as a subtle interplay between molecules and underlying substrates, remains elusive. In this work, by a combination of scanning tunneling microscopy imaging and density functional theory calculations, we report the influence of molecular chemisorption direction on the reaction selectivity of two types of dehalogenative coupling on Au(111), i.e., polymerization and cyclization, at the atomic level. The diffusion step of a reactive dehalogenated intermediate in two different chemisorption directions was theoretically revealed to be the key to determining the corresponding reaction selectivity. Our results highlight the important role of molecular chemisorption directions in regulating the on-surface dehalogenative coupling reaction pathways and products, which provides fundamental insights into the control of reaction selectivity by exploiting some subtle interfacial parameters in on-surface reactions for the fabrication of target low-dimensional carbon nanostructures.

KEYWORDS: reaction selectivity, chemisorption direction, dehalogenative coupling reaction, scanning tunneling microscopy, density functional theory
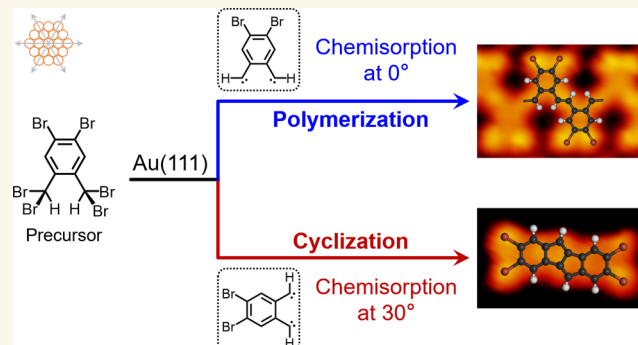
Controlling the selectivity of parallel reactions to generate desired reaction products has long been the goal of pursuit in chemistry.[1,2] To achieve this, it is essential to tailor small differences involved in the molecular systems to direct a specific reaction channel that is energetically more favorable, which requires molecular- or even atomic-level insights into the reaction mechanisms and key influencing factors for such a preference.[2] In this regard, molecule−substrate systems under ultrahigh-vacuum (UHV) conditions provide an ideal playground, along with a delicate combination with the advanced scanning probe microscopy,[3,4] which allows atomic-scale visualization of reaction intermediate states and products[5−12] as well as identification of intermolecular interactions[13−16] in an interference-free experimental environment. Based on these well-defined molecule−substrate model systems, influencing factors concerning molecular precursors, underlying substrates, and their interfacial properties that govern multipath reaction

schemes have been elucidated.[17−19] Generally, these factors correlate with the height of the energy barriers of reactions and can be fine-tuned to achieve the selection of the target on-surface reaction pathways, including activation of target functional groups, diffusion, and intermolecular coupling or intramolecular reaction as fundamental processes.[5,20] Regarding the molecular factors, the design and functionalization,[21−24] preassembly of molecular precursors,[25,26] and control of their kinetics and thermodynamics[27−29,31] have
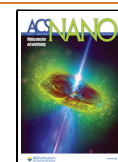
Scheme 1. Reaction Selection between Polymerization and Cyclization on Au(111) at 0 and 30°, Respectively, Based on the HBX Precursor, Which Was Theoretically Found to be Related to the Chemisorption Direction of the Dehalogenated Radical 2; the Chemisorption Directions of 0 and 30° Are Defined as the Angles between the Line along the Ortho-Bromo Substituents (Indicated by the Gray Dashed Arrow above the Two Circled Br Substituents) and the Close-Packed Directions of the Au(111) Substrate (Indicated by the Gray Arrows at the Upper Left)
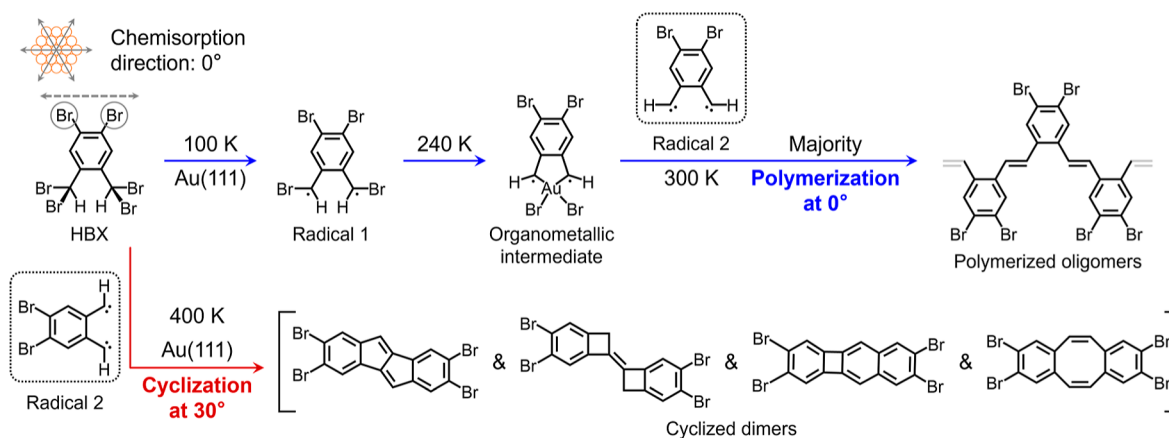
been extensively verified to be crucial for reaction selectivity. In addition, variation of the types and lattices of the underlying substrates[32−34] and the introduction of extrinsic components to provide template effects or additional intermolecular interactions[35−38] have also been widely shown to be effective. More recently, interfacial properties, such as the molecular adsorption configuration[39] and chemisorption[40] on surfaces, have presented their potential to regulate reaction selectivity in molecule−substrate systems. However, the influence of molecular chemisorption direction (i.e., different registries between target molecules and the underlying substrate lattice[41] that can be judged from the direction of specific molecular axes) on reaction selectivity remains elusive, and such a subtle interplay between molecules and the underlying substrates is, to the best of our knowledge, less discussed. It is therefore of general interest to reveal the role that molecular chemisorption direction plays in the selection of different reaction pathways as it is directly related to the step of molecular diffusion,[41,42] which should provide submolecular mechanistic understandings of reaction selectivity and its dependence on the tailoring parameters.

Herein, the influence of molecular chemisorption direction on the reaction selectivity of polymerization and cyclization has been elucidated at the atomic level based on a dehalogenative coupling reaction on Au(111). The α,α,α′,α′,4,5-hexabromo-o-xylene molecule, abbreviated as HBX (cf. Scheme 1), was selected as the molecular precursor, consisting of ortho-substituted gem-dibromomethyl groups and ortho-bromo substituents as the target reactive functional groups (to produce C−C double-bonded structures via a sp³-to-sp²-hybridized state conversion[43]) and marker groups on Au(111), respectively. The combination of high-resolution scanning tunneling microscopy (STM) imaging and density functional theory (DFT) calculations shows that the polymerization and cyclization reactions occurred selectively on Au(111) by applying different deposition and annealing strategies, leading to the controllable construction of polymerized oligomers and cyclized dimers containing sp²-hybridized carbons, respectively (cf. Scheme 1). Such reaction selectivity was found to be correlated with the different adsorption directions of HBX-based molecular states in the

reaction pathways, which were at 0 and 30° with respect to the close-packed directions of Au(111). Furthermore, the key molecular species of both pathways was theoretically revealed to be the reactive dehalogenated intermediate (radical 2), which determined the diffusion steps at 0 and 30°, respectively, and thus the corresponding reaction selectivity. Consequently, the cyclization prevails at a high deposition temperature (∼400 K) after overcoming a higher diffusion barrier at 30° to form the thermodynamically more favorable cyclized products, while the polymerization at 0° is favored in a stepwise annealing process with a lower energy barrier. Our results reveal the crucial role of molecular chemisorption directions in regulating on-surface reaction pathways and products, which further enriches the atomic-level understandings of the interfacial tailoring parameters in the on-surface reactions and lays a foundation for the controllable preparation of target low-dimensional carbon nanostructures.

RESULTS AND DISCUSSION

Initially, the HBX molecule was deposited onto the Au(111) substrate held at ∼100 K, leading to the formation of ordered ribbon-like self-assembled structures (Figure 1a). From the close-up STM image (Figure 1b), the trapezoidal morphology of an individual molecule with four bright protrusions at the vertices is identified, as depicted by the blue dotted contours. The adjacent molecules are closely packed in an antiparallel head-to-tail arrangement, forming a single molecular chain separated by interchain dark dots. Based on the DFT calculations, the debromination process of an intact HBX molecule (with the ortho-substituted gem-dibromomethyl groups) on Au(111) is calculated to be highly exothermic with no energy barrier (see Figure S1 and more details in the Supporting Information), which accords well with our previous report that the first-step debromination of the gem-dibromomethyl group has a negligible energy barrier of ∼0.16 eV on Au(111).[43] This suggests that such a process can take place when the HBX molecules are adsorbed on Au(111) at lower than room temperature (RT, ∼300 K). Thus, the trapezoidal morphology and the interchain dots are tentatively attributed to the radical 1 formed by the first-step debromination on both gem-dibromomethyl groups and the
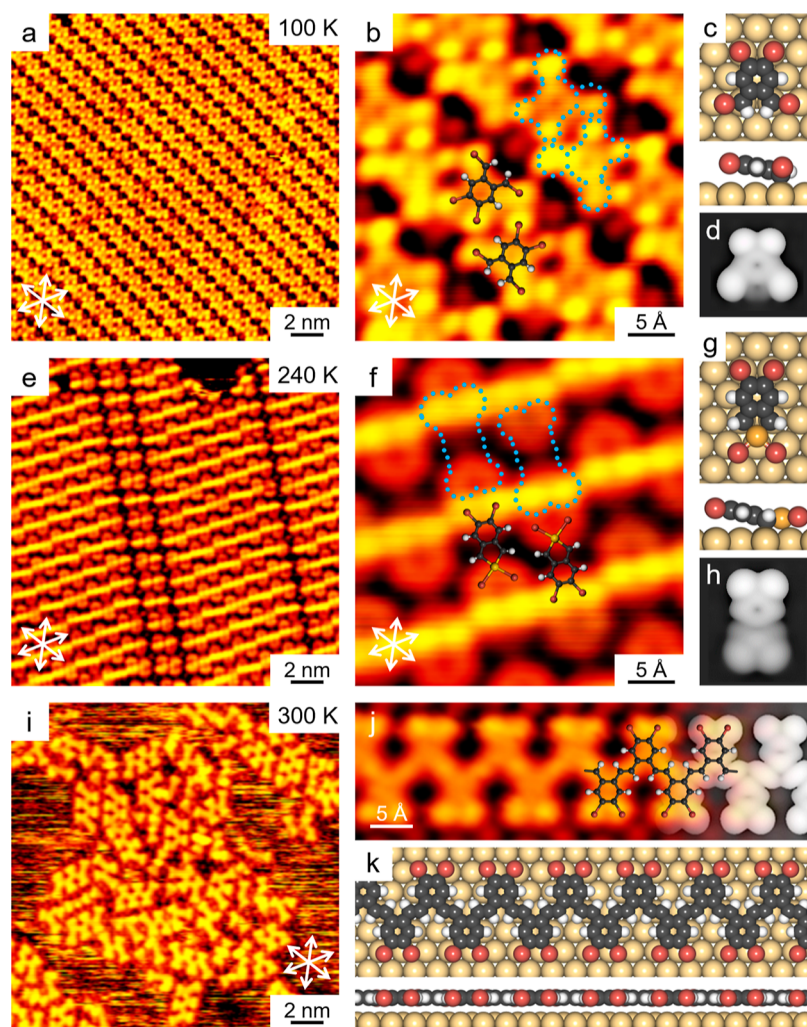
Figure 1. Polymerization process at 0° obtained by depositing the HBX molecule onto a Au(111) substrate held at ~100 K followed by stepwise annealing. (a) Large-scale and (b) close-up STM images showing the formation of radical 1 (with the coexistence of dissociated Br atoms) after the deposition of HBX onto Au(111) at 100 K. The morphologies of radical 1 are depicted by the blue dotted contours and overlaid with the DFT-optimized models. (c) Top and side views of the DFT-optimized structural model of radical 1 and (d) corresponding STM simulation. (e) Large-scale and (f) close-up STM images of the organometallic intermediates after annealing the above sample at ~240 K, which are typically depicted by the blue contours and overlaid with the DFT-optimized models. (g) Corresponding DFT-optimized structural model in top and side views and (h) STM simulation. (i) Large-scale STM image showing the construction of polymerized products in the dominant after annealing at ~300 K. (j) Magnified STM image of a polymerized chain partially superimposed with the DFT-optimized model and the STM simulation (the gray part). (k) DFT-optimized structural model of a polymerized chain in top and side views. C: black; H: white; Br: brown; Au surface atoms: yellow; Au adatom: orange. The close-packed directions of Au(111) are indicated by white arrows. Scanning conditions: $V = -1.2$ V and $I = 0.6-0.9$ nA.

dissociated Br atoms, respectively. Moreover, the adsorption direction of each molecule can also be identified, with the line along the ortho-bromo substituents parallel to the close-packed directions of the underlying Au(111) surface (i.e., defined as 0°). Accordingly, DFT calculations on the adsorption configuration of radical 1 have been performed, and the energetically most favorable structural model on Au(111) and the corresponding STM simulation are displayed in Figure 1c,d, respectively. After the first-step Br dissociation, the two remaining bromomethyl moieties directly bond to the underlying substrate, forming the surface-stabilized radical 1, while the remaining Br atoms of the bromomethyl moieties are pointed outward, resulting in the trapezoidal STM morphology. The simulated STM image nicely reproduces the experimental one, where the four bright protrusions are attributed to the Br substituents and the phenyl ring connects

them with a dark ring at the center, confirming the formation of radical 1. Notably, careful analysis of molecular domains of radical 1 on the sample confirms that radical 1 always adopts the 0° chemisorption direction (Figure S2a).

Subsequently, the above sample was gently annealed in an attempt to trigger the second-step debromination of the remaining bromomethyl moieties. After annealing at ~240 K for 30 min, a distinct self-assembled structure formed (Figure 1e). From the defects in the islands (Figure S3) and the close-up STM image (Figure 1f), the morphology of an individual molecule is distinguished, consisting of two interconnected heart-shapes with two bright and two dim protrusions on the opposite sides. By comparison with the morphology of radical 1 and similar features reported in previous reports,[34,44,45] such a molecular species is attributed to the organometallic intermediate embedded with a Au adatom, i.e., a gold–organic
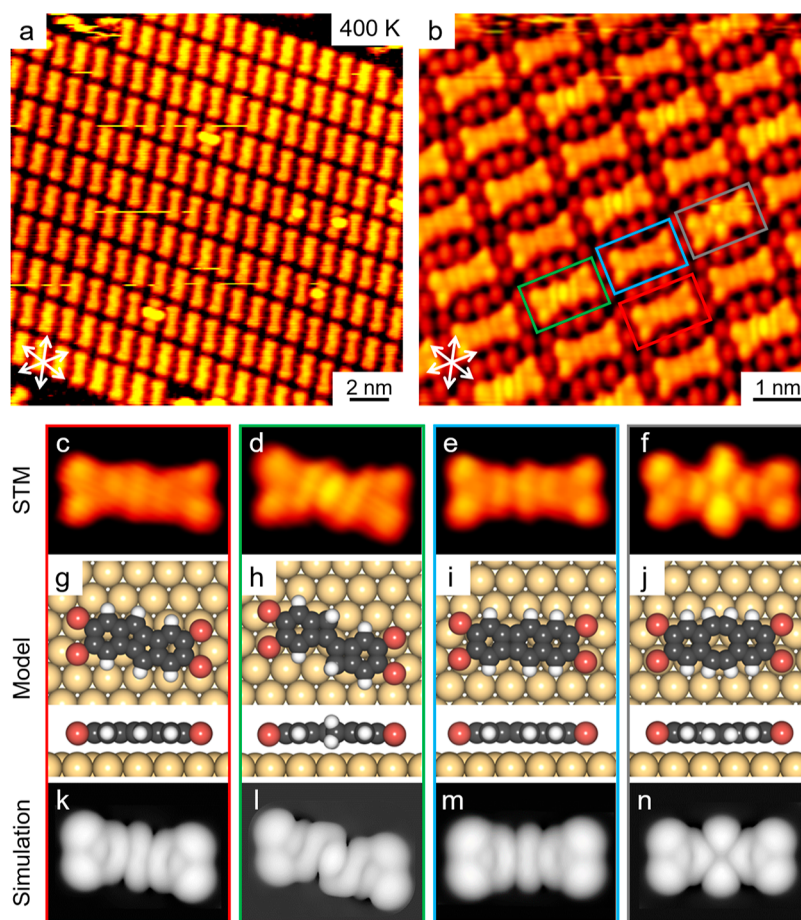
Figure 2. Cyclization products at 30° obtained by directly depositing the HBX molecule onto a Au(111) substrate held at ∼400 K. (a) Large-scale and (b) close-up STM images showing the formation of cyclized dimers after deposition of HBX onto Au(111) held at ∼400 K. (c−f) High-resolution STM images of four typical cyclized dimers, (g−j) top and side views of DFT-optimized structural models, and (k−m) corresponding STM simulations. The image sizes are 1.6 nm × 1.1 nm for (c−f). The close-packed directions of Au(111) are indicated by white arrows. Scanning conditions: (a) V = 1.2 V and I = 0.6 nA and (b−f) V = −1.2 V and I = 0.6 nA.

hybrid with AuBr₂. The DFT-optimized structural model (Figure 1g) further shows that the ortho-bromo substituents are adsorbed apparently higher than the two Br atoms attached to the Au adatom, resulting in the much brighter feature in the simulated STM image (Figure 1h), which is in good accordance with the experimental observation. Moreover, similar to the situation of radical 1, the organometallic intermediates were also found to be adsorbed at 0° in molecular domains on the sample (Figures 1e,f and S2b).

Then, the sample was further annealed at ∼300 K for 10 h, leading to the formation of less-ordered covalent structures on Au(111) via intermolecular coupling reactions (Figure 1i). Among them, polymerized oligomers, mainly composed of four to six molecular units (Figure S4), can be recognized based on their characteristic alternating morphology, as shown in the submolecularly resolved STM image (Figure 1j), where the heart-shaped moieties with two bright Br protrusions are aligned in a zigzag way along the backbone. Such a feature thus suggests the construction of C−C double bonds at the connection,[23,43] and the molecular moieties are in a trans-configuration. The corresponding DFT-optimized structural model (Figure 1k) and STM simulation (the gray part in Figure 1j) show good agreement with the experimental one in both periodicity and molecular morphology, confirming such an assignment. To have an overview of the reaction products

after annealing at ∼300 K, extensive statistics on their distribution and adsorption directions were carried out based on more than 7000 molecular units distributed in different regions of the sample. It turned out that the polymerized oligomers or chains account for approximately 70% of the total molecular units, which mainly adopted the 0° adsorption direction on the surface, with the coexistence of some unidentified motifs. Accordingly, based on the stepwise annealing strategy to ∼300 K, the dominance of the polymerized products adsorbed at 0° was achieved by the evolution from radical 1 to the organometallic intermediate adsorbed at 0°. Note that direct deposition of HBX molecules onto a Au(111) substrate held at ∼300 K also resulted in the dominance of the polymerized products (Figure S5), indicating that it is the temperature, rather than the molecular preassembly, that influences the reaction selectivity of polymerization in this case.

In contrast, after deposition of the HBX molecule onto the Au(111) substrate held at ∼400 K, dimer structures were found to be selectively formed instead of polymerized products (Figure 2a). In a special tip state, four typical molecular morphologies of dimers can be clearly distinguished as depicted by the colored rectangles in Figure 2b, coexisting with intermolecular dissociated Br atoms. These dimers share similar features at both ends while having distinct connections
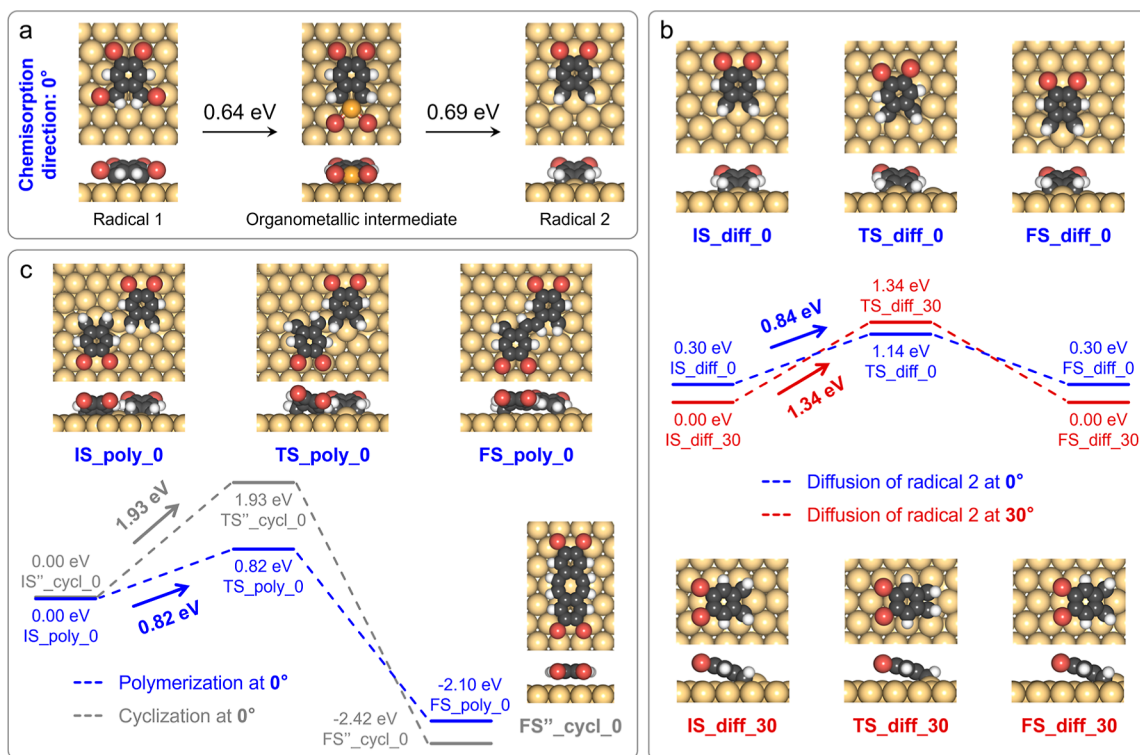
Figure 3. DFT-calculated reaction pathways of (a) debromination from radical 1 through the organometallic intermediate to radical 2 at 0°, (b) diffusion of radical 2 adsorbed at 0 and 30°, and (c) polymerization and cyclization of radical 2 adsorbed at 0°. The structural models of the initial states (IS), transition states (TS), and final states (FS) are displayed along the reaction pathways. The energies in (b) are provided with respect to that of IS_diff_30, and those in (c) are provided with respect to those of the corresponding IS. The energy barriers of the rate-limiting steps in each process are marked with arrows.

between two molecular components. It is also noteworthy that all the dimers adopt the 30° adsorption direction, which is contrary to the case shown in Figure 1. According to the previous reports,[23,43] the ortho-substituted gem-dibromomethyl groups can form four kinds of typical cyclized dimers at high temperatures of 420 K, with five-, four-, six-, or eight-membered rings embedded, respectively, which were characterized and confirmed by both STM and noncontact atomic force microscopy. Therefore, it is reasonable to suppose the formation of similar dimer structures in our case. Based on the distinct features of four dimers in the submolecularly resolved STM images (Figure 2c−f) and the above indications, DFT calculations were performed on the structural models on Au(111) (Figure 2g−j) and the corresponding STM simulations (Figure 2k−n), which are in line with the experimental ones. For instance, both the double five-membered ring connection (Figure 2c,g,k) and the double four-membered ring connection linked by a C−C double bond (Figure 2d,h,l) produce symmetric morphologies, with different offsets between two molecular components, and a prominent bright lobe is visible at the connection in the latter case. In addition, as for the connections of four- and six-membered rings (Figure 2e,i,m) and an eight-membered ring (Figure 2f,j,n), two molecular components are in a line, with two bright lobes appearing at the center in the latter case. Therefore, cyclization occurred in the 30° adsorption direction with high selectivity by the hot deposition way.

By applying different deposition and annealing strategies, polymerized oligomers and cyclized dimers have been obtained with high selectivity in a specific adsorption direction of 0 and 30°, respectively, suggesting that the adsorption directions may

be a key factor influencing the reaction selectivity. To figure out their correlations and unravel the atomic-level reaction processes, extensive DFT calculations were performed on the reaction pathways and energy barriers, as well as the stabilities of all the molecular species in different adsorption directions.

For the polymerization pathway, deposition of HBX onto Au(111) held at ∼100 K led to the formation of radical 1 via the first-step debromination of the gem-dibromomethyl groups (Figure S1). As for the chemisorption direction of radical 1, it adsorbs exclusively at 0° as determined from STM images, which is calculated to be energetically much more favorable than the situation at 30° by ∼0.56 eV (see more details in Table S1). As the next step, the transformation from radical 1 at 0° to the organometallic intermediate at 0° was experimentally captured at ∼240 K. Three dominant processes were further calculated, i.e., insertion of a Au adatom, further debromination of the remaining gem-bromomethyl groups, and recombination of Br atoms and Au to form the AuBr$_2$ moiety (Figure S6). During this process, the rate-limiting step is the debromination after the Au insertion, with an energy barrier of ∼0.64 eV (Figures 3a and S6). Note that the organometallic intermediate adsorbed at 0° is also energetically more favorable than that adsorbed at 30° by ∼0.38 eV (Table S1), in agreement with the experimental result. Besides, the diffusion of the organometallic intermediate was observed during scanning at ∼150 K (Figure S7), which is supported by the energy barrier calculation (Figure S8). Then, debromination from the AuBr$_2$ moiety of the organometallic intermediate took place, followed by removal of the Au adatom, with a total energy barrier of ∼0.69 eV, forming the reactive radical 2 at 0° for further coupling (Figures 3a and S9). As such a
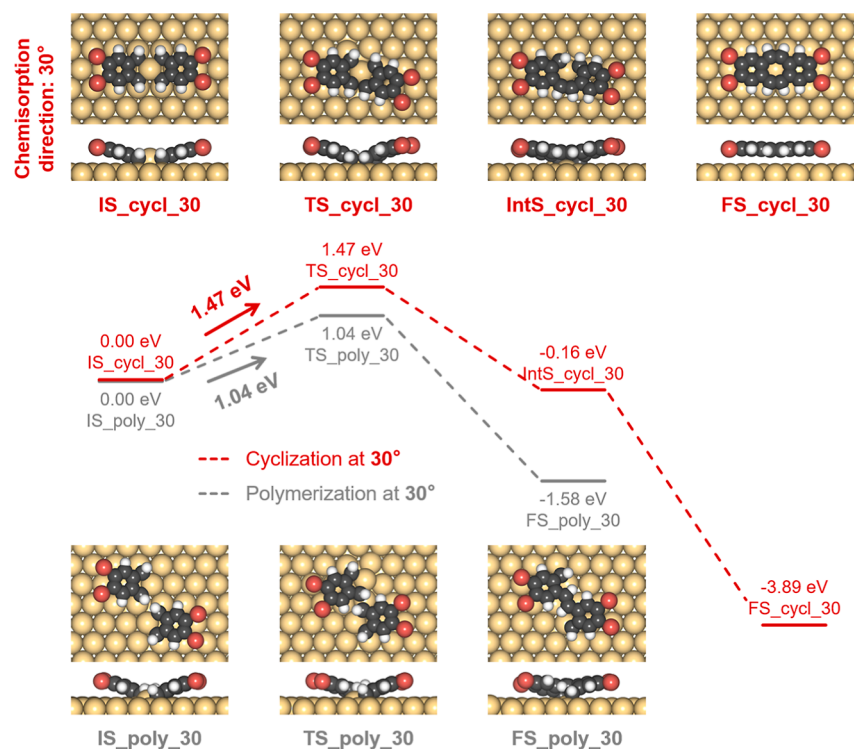
Figure 4. DFT-calculated reaction pathways of cyclization and polymerization of radical 2 adsorbed at 30°. The structural models of the IS, TS, IntS, and FS are displayed, and their energies are provided with respect to that of the corresponding IS. The energy barriers of the rate-limiting steps in each step are marked with arrows.

transformation process is highly endothermic, it is difficult to capture radical 2 in experiments (the reverse process to the organometallic intermediate would be preferred). Interestingly, radical 2 chemisorbed at 0° on Au(111) is calculated to be less stable than that at 30° by ∼0.30 eV (Table S1), in contrast to the cases of radical 1 and the organometallic intermediate. It is also worth noting that the energy barriers for the interconversion between these two chemisorbed states are calculated to be ∼0.28 and ∼0.58 eV for rotation from 0 to 30° and from 30 to 0° (Figure S10), respectively, lower than that of the formation of radical 2 (∼0.69 eV). Thus, once radical 2 is formed at 0°, it tends to rotate by 30° to reach the energetically more stable state.

Subsequently, the diffusion of the radical 2 is a prerequisite for the intermolecular coupling reactions, which require two radicals to approach close enough to each other. Significantly, the more stable radical 2 at 30° suffers from a high diffusion barrier of ∼1.34 eV (red lines in Figure 3b), which severely hinders further intermolecular coupling at mild reaction temperatures. On the contrary, the diffusion of the less stable radical 2 at 0° requires an energy barrier of only ∼0.84 eV, which is much more rational with respect to the experimental observation of coupled products at ∼300 K. Thereafter, based on radical 2 at 0°, the reaction selectivity between polymerization and cyclization was theoretically explored, and the reaction pathways to form the polymerized dimer and the cyclized dimer embedded with an eight-membered ring were calculated to simplify the system, respectively. Note that the other cyclized dimer structures may be transformed from the one with an eight-membered ring connection by on-surface rearrangement reactions and dehydrogenation,[46,47] which is applied as the typical cyclized dimer for transition-state calculations. Consequently, the energy barrier for two radicals

2 at 0° (in a shoulder-to-shoulder manner) to form the polymerized dimer is only ∼0.82 eV (Figure 3c), which is almost identical to that of its diffusion and is reasonable for the successful polymerization at ∼300 K. In contrast, the energy barrier for two radicals 2 at 0° (in a face-to-face manner) to cyclize is calculated to be much higher, i.e., ∼2.26 eV (Figure S11a), which can be slightly reduced to ∼2.17 and ∼1.93 eV with the help of one (Figure S11b) and two Au adatoms (Figure S11c), respectively. Thus, the differences in reaction barriers between the two reaction pathways rationalize the preference for polymerization at ∼300 K from the viewpoint of kinetics.

For the cyclization pathway, deposition of HBX onto Au(111) held at ∼400 K resulted in the direct construction of cyclized dimers, suggesting the formation of radical 2 by the complete debromination of gem-dibromomethyl groups upon deposition. Moreover, the high diffusion barrier of ∼1.34 eV for the more stable radical 2 at 30° can also be overcome at such a high temperature. Consequently, radical 2 at 30° should be responsible for the further coupling processes. Based on two radicals 2 at 30°, the energy barrier for them to form the polymerized dimer is ∼1.04 eV (gray lines in Figure 4), while the energy barrier of cyclization is determined to be ∼1.47 eV (red lines in Figure 4) and can be slightly reduced to ∼1.40 eV with the assistance of two Au adatoms (Figure S12). As the barrier of cyclization is comparable to that of diffusion and higher than that of polymerization, radicals 2 should be able to undergo both cyclization and polymerization after overcoming the diffusion barrier from a kinetic point of view. Moreover, thermodynamics also plays an important role in influencing the overall reaction selectivity. The comparison between the total energies of the polymerized and cyclized dimers shows that the latter one is energetically much more stable by ∼2.61 eV

(Table S2), indicating strong preference for cyclization after hot deposition. As a result, the cyclization was found to prevail at ~400 K in the experiments, indicating a thermodynamically driven process.

Based on the above experimental and theoretical results, it has been shown that the polymerization and cyclization reactions take place with high selectivity on Au(111) by applying different deposition and annealing strategies, with the controllable construction of polymerized oligomers and cyclized dimers, respectively. The reaction pathways calculated above have been further summarized in Scheme S1, where the chemisorption direction of the reactive dehalogenated radical 2 plays a crucial role in determining the corresponding reaction selectivity.

There are two types of situations described below. If intermolecular coupling reactions start with the reactants in the energetically most stable state, i.e., the radical 2 adsorbed at 30° (Table S1), the reactions can hardly occur at mild temperatures (for example, ~300 K in our experiments) due to its high diffusion barrier (~1.34 eV). Also note that the difference in the diffusion energy barrier of ~0.5 eV can significantly influence the reaction process based on the Arrhenius equation as reported,[31,48] and its impact on the corresponding reaction rates would be greatly reduced with the increase of temperature. Only when the temperature is high enough (e.g., ~400 K) for the radical 2_30° to overcome such a diffusion barrier can the polymerization and cyclization further take place. After the diffusion step, the much higher stability of the cyclized dimer than that of the polymerized one (Table S2) strongly favors the selection of cyclization over polymerization (although polymerization has a lower energy barrier), leading to the dominance of cyclized dimers upon hot deposition at ~400 K. This could be rationalized by the almost comparable energy barriers of diffusion (~1.34 eV) and cyclization (~1.47 and ~1.40 eV in the absence and presence of Au adatoms, respectively), which also indicates the crucial role of thermodynamics in influencing the reaction selectivity at high temperatures.

In contrast, at lower temperatures (e.g., ~300 K), where the diffusion (or further cyclization) barrier of the radical 2_30° cannot be easily overcome, the less stable radical 2_0° should be selected as the reactant. In this way, after such a diffusion step (~0.84 eV), the polymerization is strongly favored over the cyclization owing to its much lower energy barrier (~0.82 eV), in good agreement with the preference for polymerized products at ~300 K in STM experiments. In addition, since the deposition rate and coverage are kept constant for both strategies, the selectivity in the reaction products is not related to the different sublimation parameters. Besides, the influence of Br adatoms on the reaction selectivity of polymerization and cyclization has also been investigated, which was found to be negligible in this study (see more details in Figure S13). In short, the reaction selectivity between polymerization and cyclization is significantly influenced by both the diffusion and coupling barriers of radical 2 at two chemisorption directions (i.e., 0 and 30°) and the total energies of the step-by-step products. It is also noteworthy that the energy barriers (e.g., diffusion and coupling in this case) vary widely according to different chemisorption directions, which may also induce the reversion of reaction preference in some other on-surface molecular systems and further bring huge influences on the reaction selectivity.

For on-surface reactions, several previous reports have revealed that the reaction selectivity depends critically on the substrate temperatures during deposition,[27−31] which are generally attributed to the reaction kinetics, leaving the atomic-level processes elusive. Herein, our experimental and theoretical results highlight the significant role of molecular chemisorption directions played in the on-surface reactions and syntheses, especially reevaluating the influence of an unfavorable chemisorption direction and state in reaction pathways and products. More importantly, it provides fundamental insights into the regulation of reaction selectivity by exploiting some subtle interfacial parameters in the on-surface reactions.

CONCLUSIONS

In summary, by a combination of STM imaging and DFT calculations, we reveal the influence of molecular chemisorption direction on the reaction selectivity of polymerization and cyclization at the atomic level, which is based on a dehalogenative coupling reaction on Au(111). The polymerized and cyclized products were selectively formed at specific adsorption directions (i.e., 0 and 30°, respectively) by applying different deposition and annealing strategies. Moreover, the chemisorption direction of the reactive dehalogenated radical 2 and the corresponding diffusion step in the two different directions were theoretically revealed to be the key to determining the reaction selectivity. Our results enrich the submolecular mechanistic understandings of the influencing factors involved in on-surface reactions and should facilitate the control of reaction selectivity to synthesize the desired nanostructures.

METHODS

All the STM experiments were performed in a UHV chamber (with a base pressure of ~1.0 × 10^{-10} mbar), equipped with a variable-temperature, fast-scanning "Aarhus-type" STM using electrochemically etched W tips.[49,50] The Au(111) substrate was cleaned by Ar$^+$-ion sputtering and annealing at ~800 K for repeated cycles. After thorough degassing, the $\alpha,\alpha,\alpha',\alpha'$,4,5-hexabromo-o-xylene molecule (abbreviated as HBX, purchased from Macklin, with a purity of >98%) was sublimated by a homemade Knudsen cell at ~390 K with the duration time within 2 min in the preparation chamber. Thereafter, the sample was transferred within the UHV chamber to the STM head for scanning. All the STM images were recorded at 100−150 K and were further smoothed to eliminate noises.

The calculations were performed in the framework of DFT by using the Vienna Ab initio Simulation Package (VASP).[51,52] The projector-augmented wave method was used to describe the interaction between ions and electrons.[53,54] The Perdew−Burke−Ernzerhof generalized gradient approximation exchange−correlation functional was employed,[55] and van der Waals interactions were included using the dispersion-corrected DFT-D3 method of Grimme.[56] The atomic structures were relaxed using the conjugate gradient algorithm scheme, as implemented in the VASP code until the forces on all unconstrained atoms were ≤0.03 eV/Å. Plane waves were used as a basis set with an energy cutoff of 400 eV. For the structural models involved in the cyclization processes, the Au(111) substrate was modeled by a four-layered slab separated by a vacuum region of ~15 Å, with the bottom two layers fixed. For all the other structural models, the Au(111) substrate was modeled by three-layered slabs, where the bottom one layer was fixed. Simulated STM images were obtained based on the Tersoff−Hamann method.[57,58] Reaction pathways were calculated by a combination of the climbing image-nudged elastic band (CI-NEB)[59] and dimer methods.[60] The CI-NEB method was used to find an initial guess of a transition state,

which was then refined by the dimer method until the forces acting on the path typically converged to ≤0.03 eV/Å.

ASSOCIATED CONTENT

Ⓢ Supporting Information

The Supporting Information is available free of charge at https://pubs.acs.org/doi/10.1021/acsnano.4c02766.

> Additional STM images of radical 1 and the organometallic intermediate, DFT calculations on the reaction pathways and structural models, and schematic illustration summarizing all the reaction pathways (PDF)

AUTHOR INFORMATION

Corresponding Authors

Chi Zhang − *Interdisciplinary Materials Research Center, School of Materials Science and Engineering, Tongji University, Shanghai 201804, People's Republic of China;* ⓞ orcid.org/0000-0002-2335-4579; Email: zhangchi11@tongji.edu.cn

Yousoo Kim − *Surface and Interface Science Laboratory, RIKEN, Wako, Saitama 351-0198, Japan;* ⓞ orcid.org/0000-0001-7730-0704; Email: ykim@riken.jp

Wei Xu − *Interdisciplinary Materials Research Center, School of Materials Science and Engineering, Tongji University, Shanghai 201804, People's Republic of China;* ⓞ orcid.org/0000-0003-0216-794X; Email: xuwei@tongji.edu.cn

Authors

Zewei Yi − *Interdisciplinary Materials Research Center, School of Materials Science and Engineering, Tongji University, Shanghai 201804, People's Republic of China*

Zhaoyu Zhang − *Interdisciplinary Materials Research Center, School of Materials Science and Engineering, Tongji University, Shanghai 201804, People's Republic of China*

Yuan Guo − *Interdisciplinary Materials Research Center, School of Materials Science and Engineering, Tongji University, Shanghai 201804, People's Republic of China*

Yuhong Gao − *Interdisciplinary Materials Research Center, School of Materials Science and Engineering, Tongji University, Shanghai 201804, People's Republic of China*

Rujia Hou − *Interdisciplinary Materials Research Center, School of Materials Science and Engineering, Tongji University, Shanghai 201804, People's Republic of China*

Complete contact information is available at:
https://pubs.acs.org/10.1021/acsnano.4c02766

Author Contributions

The manuscript was written through contributions of all authors. All authors have given approval to the final version of the manuscript.

Notes

The authors declare no competing financial interest.

ACKNOWLEDGMENTS

REFERENCES

(1) Zhou, W.; Cheng, K.; Kang, J.; Zhou, C.; Subramanian, V.; Zhang, Q.; Wang, Y. New Horizon in C1 Chemistry: Breaking the Selectivity Limitation in Transformation of Syngas and Hydrogenation of CO_2 into Hydrocarbon Chemicals and Fuels. *Chem. Soc. Rev.* **2019**, *48*, 3193−3228.

(2) Somorjai, G. A.; Park, J. Y. Molecular Factors of Catalytic Selectivity. *Angew. Chem., Int. Ed.* **2008**, *47*, 9212−9228.

(3) Pavliček, N.; Gross, L. Generation, Manipulation and Characterization of Molecules by Atomic Force Microscopy. *Nat. Rev. Chem* **2017**, *1* (1), 0005.

(4) Bian, K.; Gerber, C.; Heinrich, A. J.; Müller, D. J.; Scheuring, S.; Jiang, Y. Scanning Probe Microscopy. *Nat. Rev. Methods Primers* **2021**, *1*, 36.

(5) Grill, L.; Hecht, S. Covalent On-Surface Polymerization. *Nat. Chem.* **2020**, *12*, 115−130.

(6) Shen, Q.; Gao, H.; Fuchs, H. Frontiers of On-Surface Synthesis: From Principles to Applications. *Nano Today* **2017**, *13*, 77−96.

(7) Talirz, L.; Ruffieux, P.; Fasel, R. On-Surface Synthesis of Atomically Precise Graphene Nanoribbons. *Adv. Mater.* **2016**, *28*, 6222−6231.

(8) Zhang, C.; Yi, Z.; Xu, W. Scanning Probe Microscopy in Probing Low-Dimensional Carbon-Based Nanostructures and Nanomaterials. *Mater. Futures* **2022**, *1*, 032301.

(9) Yang, B.; Dong, B.; Chi, L. On-Surface Intramolecular Reactions. *ACS Nano* **2020**, *14*, 6376−6382.

(10) Song, S.; Su, J.; Telychko, M.; Li, J.; Li, G.; Li, Y.; Su, C.; Wu, J.; Lu, J. On-Surface Synthesis of Graphene Nanostructures with π-Magnetism. *Chem. Soc. Rev.* **2021**, *50*, 3238−3262.

(11) Zhang, C.; Kazuma, E.; Kim, Y. Atomic-Scale Visualization of the Stepwise Metal-Mediated Dehalogenative Cycloaddition Reaction Pathways: Competition Between Radicals and Organometallic Intermediates. *Angew. Chem., Int. Ed.* **2019**, *58*, 17736−17744.

(12) Zhang, C.; Jaculbia, R. B.; Tanaka, Y.; Kazuma, E.; Imada, H.; Hayazawa, N.; Muranaka, A.; Uchiyama, M.; Kim, Y. Chemical Identification and Bond Control of π-Skeletons in a Coupling Reaction. *J. Am. Chem. Soc.* **2021**, *143*, 9461−9467.

(13) Dong, L.; Gao, Z.; Lin, N. Self-Assembly of Metal-Organic Coordination Structures on Surfaces. *Prog. Surf. Sci.* **2016**, *91*, 101−135.

(14) Zhang, C.; Xu, W. Interactions Between Water and Organic Molecules or Inorganic Salts on Surfaces. *Aggregate* **2022**, *3*, No. e175.

(15) Xie, L.; Ding, Y.; Li, D.; Zhang, C.; Wu, Y.; Sun, L.; Liu, M.; Qiu, X.; Xu, W. Local Chiral Inversion of Thymine Dimers by Manipulating Single Water Molecules. *J. Am. Chem. Soc.* **2022**, *144*, 5023−5028.

(16) Yi, Z.; Guo, Y.; Hou, R.; Zhang, Z.; Gao, Y.; Zhang, C.; Xu, W. Revealing the Orientation Selectivity of Tetrapyridyl-Substituted Porphyrins Constrained in Molecular "Klotski Puzzles. *J. Am. Chem. Soc.* **2023**, *145*, 22366−22373.

(17) Clair, S.; de Oteyza, D. G. Controlling a Chemical Coupling Reaction on a Surface: Tools and Strategies for On-Surface Synthesis. *Chem. Rev.* **2019**, *119*, 4717−4776.

(18) Wang, T.; Zhu, J. Confined On-Surface Organic Synthesis: Strategies and Mechanisms. *Surf. Sci. Rep.* **2019**, *74*, 97−140.

(19) Zhou, X.; Dai, J.; Wu, K. Steering On-Surface Reactions with Self-Assembly Strategy. *Phys. Chem. Chem. Phys.* **2017**, *19*, 31531−31539.

(20) Björk, J.; Hanke, F.; Stafstrom, S. Mechanisms of Halogen-Based Covalent Self-Assembly on Metal Surfaces. *J. Am. Chem. Soc.* **2013**, *135*, 5768−5775.

(21) Li, D.; Qiu, X.; Li, S.; Ren, Y.; Zhu, Y.; Shu, C.; Hou, X.; Liu, M.; Shi, X.; Qiu, X.; Liu, P. Ladder Phenylenes Synthesized on

Au(111) Surface *via* Selective [2 + 2] Cycloaddition. *J. Am. Chem. Soc.* **2021**, *143*, 12955−12960.

(22) Fan, Q.; Werner, S.; Tschakert, J.; Ebeling, D.; Schirmeisen, A.; Hilt, G.; Hieringer, W.; Gottfried, J. M. Precise Monoselective Aromatic C-H Bond Activation by Chemisorption of *Meta*-Aryne on a Metal Surface. *J. Am. Chem. Soc.* **2018**, *140*, 7526−7532.

(23) Tang, Y.; Ejlli, B.; Niu, K.; Li, X.; Hao, Z.; Xu, C.; Zhang, H.; Rominger, F.; Freudenberg, J.; Bunz, U. H. F.; Muellen, K.; Chi, L. On-Surface Debromination of 2,3-Bis(dibromomethyl)- and 2,3-Bis(bromomethyl)naphthalene: Dimerization or Polymerization? *Angew. Chem.* **2022**, *134*, No. e202204123.

(24) Wang, T.; Lv, H.; Fan, Q.; Feng, L.; Wu, X.; Zhu, J. Highly Selective Synthesis of *cis*-Enediynes on a Ag(111) Surface. *Angew. Chem., Int. Ed.* **2017**, *56*, 4762−4766.

(25) Chen, Q.; Cramer, J. R.; Liu, J.; Jin, X.; Liao, P.; Shao, X.; Gothelf, K. V.; Wu, K. Steering On-Surface Reactions by a Self-Assembly Approach. *Angew. Chem., Int. Ed.* **2017**, *56*, 5026−5030.

(26) Zhang, C.; Sun, Q.; Chen, H.; Tan, Q.; Xu, W. Formation of Polyphenyl Chains Through Hierarchical Reactions: Ullmann Coupling Followed by Cross-Dehydrogenative Coupling. *Chem. Commun.* **2015**, *51*, 495−498.

(27) Fritton, M.; Duncan, D. A.; Deimel, P. S.; Rastgoo-Lahrood, A.; Allegretti, F.; Barth, J. V.; Heckl, W. M.; Björk, J.; Lackinger, M. The Role of Kinetics versus Thermodynamics in Surface-Assisted Ullmann Coupling on Gold and Silver Surfaces. *J. Am. Chem. Soc.* **2019**, *141*, 4824−4832.

(28) Eichhorn, J.; Nieckarz, D.; Ochs, O.; Samanta, D.; Schmittel, M.; Szabelski, P. J.; Lackinger, M. On-Surface Ullmann Coupling: The Influence of Kinetic Reaction Parameters on the Morphology and Quality of Covalent Networks. *ACS Nano* **2014**, *8*, 7880−7889.

(29) Kawai, S.; Takahashi, K.; Ito, S.; Pawlak, R.; Meier, T.; Spijker, P.; Canova, F. F.; Tracey, J.; Nozaki, K.; Foster, A. S.; Meyer, E. Competing Annulene and Radialene Structures in a Single Anti-Aromatic Molecule Studied by High-Resolution Atomic Force Microscopy. *ACS Nano* **2017**, *11*, 8122−8130.

(30) Cirera, B.; Giménez-Agulló, N.; Björk, J.; Martínez-Peña, F.; Martin-Jimenez, A.; Rodriguez-Fernandez, J.; Pizarro, A. M.; Otero, R.; Gallego, J. M.; Ballester, P.; Galan-Mascaros, J. R.; Ecija, D. Thermal Selectivity of Intermolecular versus Intramolecular Reactions on Surfaces. *Nat. Commun.* **2016**, *7*, 11002.

(31) Wang, T.; Huang, J.; Lv, H.; Fan, Q.; Feng, L.; Tao, Z.; Ju, H.; Wu, X.; Tait, S. L.; Zhu, J. Kinetic Strategies for the Formation of Graphyne Nanowires *via* Sonogashira Coupling on Ag(111). *J. Am. Chem. Soc.* **2018**, *140*, 13421−13428.

(32) Liu, J.; Chen, Q.; Xiao, L.; Shang, J.; Zhou, X.; Zhang, Y.; Wang, Y.; Shao, X.; Li, J.; Chen, W.; Xu, G.; Tang, H.; Zhao, D.; Wu, K. Lattice-Directed Formation of Covalent and Organometallic Molecular Wires by Terminal Alkynes on Ag Surfaces. *ACS Nano* **2015**, *9*, 6305−6314.

(33) Li, Q.; Yang, B.; Lin, H.; Aghdassi, N.; Miao, K.; Zhang, J.; Zhang, H.; Li, Y.; Duhm, S.; Fan, J.; Chi, L. Surface-Controlled Mono/Diselective *ortho* C-H Bond Activation. *J. Am. Chem. Soc.* **2016**, *138*, 2809−2814.

(34) Zhong, Q.; Niu, K.; Chen, L.; Zhang, H.; Ebeling, D.; Björk, J.; Müllen, K.; Schirmeisen, A.; Chi, L. Substrate-Modulated Synthesis of Metal-Organic Hybrids by Tunable Multiple Aryl-Metal Bonds. *J. Am. Chem. Soc.* **2022**, *144*, 8214−8222.

(35) Xing, S.; Zhang, Z.; Fei, X.; Zhao, W.; Zhang, R.; Lin, T.; Zhao, D.; Ju, H.; Xu, H.; Fan, J.; Zhu, J.; Ma, Y.; Shi, Z. Selective On-Surface Covalent Coupling Based on Metal-Organic Coordination Template. *Nat. Commun.* **2019**, *10*, 70.

(36) Zhang, X.; Xue, N.; Li, C.; Li, N.; Wang, H.; Kocić, N.; Beniwal, S.; Palotás, K.; Li, R.; Xue, Q.; Maier, S.; Hou, S.; Wang, Y. Coordination-Controlled C-C Coupling Products via ortho-Site C-H Activation. *ACS Nano* **2019**, *13*, 1385−1393.

(37) Zhang, C.; Kazuma, E.; Kim, Y. Steering the Reaction Pathways of Terminal Alkynes by Introducing Oxygen Species: From C-C Coupling to C-H Activation. *J. Am. Chem. Soc.* **2022**, *144*, 10282−10290.

(38) Liu, X.; Matěj, A.; Kratky, T.; Mendieta-Moreno, J. I.; Günther, S.; Mutombo, P.; Decurtins, S.; Aschauer, U.; Repp, J.; Jelinek, P.; Liu, S.; Patera, L. L. Exploiting Cooperative Catalysis for the On-Surface Synthesis of Linear Heteroaromatic Polymers *via* Selective C-H Activation. *Angew. Chem., Int. Ed.* **2022**, *61*, No. e202112798.

(39) Wang, J.; Niu, K.; Xu, C.; Zhu, H.; Ding, H.; Han, D.; Zheng, Y.; Xi, J.; You, S.; Deng, C.; Lin, H.; Rosen, J.; Zhu, J.; Björk, J.; Li, Q.; Chi, L. Influence of Molecular Configurations on the Desulfonylation Reactions on Metal Surfaces. *J. Am. Chem. Soc.* **2022**, *144*, 21596−21605.

(40) Zeng, Z.; Guo, D.; Wang, T.; Chen, Q.; Matěj, A.; Huang, J.; Han, D.; Xu, Q.; Zhao, A.; Jelínek, P.; de Oteyza, D. G.; McEwen, J.; Zhu, J. Chemisorption-Induced Formation of Biphenylene Dimer on Ag(111). *J. Am. Chem. Soc.* **2022**, *144*, 723−732.

(41) Otero, R.; Hümmelink, F.; Sato, F.; Legoas, S. B.; Thostrup, P.; Lægsgaard, E.; Stensgaard, I.; Galvão, D. S.; Besenbacher, F. Lock-and-Key Effect in the Surface Diffusion of Large Organic Molecules Probed by STM. *Nat. Mater.* **2004**, *3*, 779−782.

(42) Rotter, P.; Lechner, B. A. J.; Morherr, A.; Chisnall, D. M.; Ward, D. J.; Jardine, A. P.; Ellis, J.; Allison, W.; Eckhardt, B.; Witte, G. Coupling Between Diffusion and Orientation of Pentacene Molecules on an Organic Surface. *Nat. Mater.* **2016**, *15*, 397−400.

(43) Cai, L.; Yu, X.; Liu, M.; Sun, Q.; Bao, M.; Zha, Z.; Pan, J.; Ma, H.; Ju, H.; Hu, S.; Xu, L.; Zou, J.; Yuan, C.; Jacob, T.; Björk, J.; Zhu, J.; Qiu, X.; Xu, W. Direct Formation of C-C Double-Bonded Structural Motifs by On-Surface Dehalogenative Homocoupling of *gem*-Dibromomethyl Molecules. *ACS Nano* **2018**, *12*, 7959−7966.

(44) Zuzak, R.; Brandimarte, P.; Olszowski, P.; Izydorczyk, I.; Markoulides, M.; Such, B.; Kolmer, M.; Szymonski, M.; Garcia-Lekue, A.; Sánchez-Portal, D.; Gourdon, A.; Godlewski, S. On-Surface Synthesis of Chlorinated Narrow Graphene Nanoribbon Organometallic Hybrids. *J. Phys. Chem. Lett.* **2020**, *11*, 10290−10297.

(45) Liu, M.; Liu, M.; She, L.; Zha, Z.; Pan, J.; Li, S.; Li, T.; He, Y.; Cai, Z.; Wang, J.; Zheng, Y.; Qiu, X.; Zhong, D. Graphene-Like Nanoribbons Periodically Embedded with Four- and Eight-Membered Rings. *Nat. Commun.* **2017**, *8*, 14924.

(46) Pérez-Elvira, E.; Barragán, A.; Chen, Q.; Soler-Polo, D.; Sánchez-Grande, A.; Vicent, D. J.; Lauwaet, K.; Santos, J.; Mutombo, P.; Mendieta-Moreno, J. I.; de la Torre, B.; Gallego, J. M.; Miranda, R.; Martín, N.; Jelínek, P.; Urgel, J. I.; Écija, D. Generating Antiaromaticity in Polycyclic Conjugated Hydrocarbons by Thermally Selective Skeletal Rearrangements at Interfaces. *Nat. Synth.* **2023**, *2*, 1159−1170.

(47) Kawai, S.; Sang, H.; Kantorovich, L.; Takahashi, K.; Nozaki, K.; Ito, S. An Endergonic Synthesis of Single Sondheimer-Wong Diyne by Local Probe Chemistry. *Angew. Chem., Int. Ed.* **2020**, *59*, 10842−10847.

(48) Cao, N.; Björk, J.; Corral-Rascon, E.; Chen, Z.; Ruben, M.; Senge, M. O.; Barth, J. V.; Riss, A. The Role of Aromaticity in the Cyclization and Polymerization of Alkyne-Substituted Porphyrins on Au(111). *Nat. Chem.* **2023**, *15*, 1765−1772.

(49) Besenbacher, F. Scanning Tunnelling Microscopy Studies of Metal Surfaces. *Rep. Prog. Phys.* **1996**, *59*, 1737−1802.

(50) Laegsgaard, E.; Österlund, L.; Thostrup, P.; Rasmussen, P. B.; Stensgaard, I.; Besenbacher, F. A High-Pressure Scanning Tunneling Microscope. *Rev. Sci. Instrum.* **2001**, *72*, 3537−3542.

(51) Kresse, G.; Hafner, J. Ab Initio Molecular Dynamics for Open-Shell Transition Metals. *Phys. Rev. B* **1993**, *48*, 13115−13118.

(52) Kresse, G.; Furthmüller, J. Efficient Iterative Schemes for Ab Initio Total-Energy Calculations Using a Plane-Wave Basis Set. *Phys. Rev. B* **1996**, *54*, 11169−11186.

(53) Blöchl, P. E. Projector Augmented-Wave Method. *Phys. Rev. B* **1994**, *50*, 17953−17979.

(54) Kresse, G.; Joubert, D. From Ultrasoft Pseudopotentials to the Projector Augmented-Wave Method. *Phys. Rev. B* **1999**, *59*, 1758−1775.

(55) Perdew, J. P.; Burke, K.; Ernzerhof, M. Generalized Gradient Approximation Made Simple. *Phys. Rev. Lett.* **1996**, *77*, 3865−3868.

(56) Grimme, S.; Antony, J.; Ehrlich, S.; Krieg, H. A Consistent and Accurate Ab Initio Parametrization of Density Functional Dispersion Correction (DFT-D) for the 94 Elements H-Pu. *J. Chem. Phys.* **2010**, *132*, 154104.

(57) Vanpoucke, D. E. P.; Brocks, G. Formation of Pt-induced Ge Atomic Nanowires on Pt/Ge(001): A Density Functional Theory Study. *Phys. Rev. B* **2008**, *77*, 241308.

(58) Tersoff, J.; Hamann, D. R. Theory of the Scanning Tunneling Microscope. *Phys. Rev. B* **1985**, *31*, 805−813.

(59) Henkelman, G.; Uberuaga, B. P.; Jónsson, H. A Climbing Image Nudged Elastic Band Method for Finding Saddle Points and Minimum Energy Paths. *J. Chem. Phys.* **2000**, *113*, 9901−9904.

(60) Kästner, J.; Sherwood, P. Superlinearly Converging Dimer Method for Transition State Search. *J. Chem. Phys.* **2008**, *128*, 014106.